Journal of Chromatography, 626 (1992) 59–69
Elsevier Science Publishers B.V., Amsterdam

CHROM. 24 322

Flame-based thermionic detection coupled on-line with microcolumn liquid chromatography

I. Optimization of the system

Ch. E. Kientz and A. Verweij

Prins Maurits Laboratory TNO, P.O. Box 45, 2280 AA Rijswijk (Netherlands)

G. J. de Jong* and U. A. Th. Brinkman

Department of Analytical Chemistry, Free University, De Boelelaan 1083, 1081 HV Amsterdam (Netherlands)

ABSTRACT

A thermionic detector originally developed for gas chromatography was coupled with microcolumn (0.3 mm I.D.) liquid chromatography. For coupling, an interface used previously for flame photometric detection was used. Minor modifications to the burner head and detector were necessary. The eluent and analyte introduction were studied by varying parameters such as the air, hydrogen and helium gas flow-rates and the rubidium source–burner rim distance. To obtain stable eluent and analyte introduction, a minimum flame length of about 6 mm was required. A near-stoichiometric H_2:O_2 ratio was found to give optimum detector sensitivity; the optimum rubidium source–burner rim distance and hydrogen flow-rate were mutually dependent. The system was used for the determination of organophosphorus compounds, *e.g.*, the pesticide dichlorvos and its polar non-volatile metabolite dimethylphosphoric acid and the herbicide glyphosate. For the analytes tested, the detection limit was 10–20 pg/s of phosphorus.

INTRODUCTION

The on-line combination of miniaturized liquid chromatography (LC) with flow-rates of 1–50 μl/min and phosphorus-selective gas chromatographic (GC) detectors has been achieved by several groups [1–10]. In miniaturized LC coupled with thermionic detection (TID), one can distinguish between work carried out with flame-based and flameless TID. The use of flameless TID in combination with 0.7 mm I.D. packed microbore columns and an evaporation-type interface was described by Brinkman and co-workers [1–3]. In their work examples were presented of trace-level organophosphorus pesticide determinations in tomato, onion and sediment samples.

Novotny and co-workers [5,6] described the coupling of a laboratory-made dual-flame thermionic detector with micro-LC with the use of an interface based on concentric nebulization of the mobile phase solvent and solutes. In later work, nebulization was carried out orthogonally to improve the determination of larger molecules. With this approach, the nebulizing efficiency was significantly increased for larger molecules; organophosphorus species having molecular masses (M_r) of >500 could now be detected. As more (organic) effluent

Correspondence to: Professor U. A. Th. Brinkman, Department of Analytical Chemistry, Free University, De Boelelaan 1083, 1081 HV Amsterdam, Netherlands.

* Present address: Solvay Duphar BV, Analytical Development Department, P.O. Box 900, 1380 DA Weesp, Netherlands.

0021-9673/92/$05.00

was introduced into the flame compared with concentric nebulization, the flame temperature increased and an increase in background signal was observed. As a result, the detection limits remained similar to those obtained with the former version of the TID instrument. For the less volatile dimethylthiophosphinic ester of estradiol (M_r = 456) the detection limit was ten times higher than for trimethyl phosphate. A linear dynamic range of two, instead of the earlier three, decades was obtained due to a bipolar orientation at high concentrations. More recently, the same group returned to concentric nebulization and the system was optimized for nitrogen-containing species [7]. Unfortunately, no further work has been published on their micro-LC–TID coupling.

There is still a need for selective phosphorus detection in LC using an interface principle which makes the system suitable for various types of application, *i.e.*, independent of analyte volatility and/or polarity. In addition, real samples often contain non-volatile matrix compounds which make detection impossible or reduce the lifetime of systems based on evaporation owing to blocking of the heated capillary. In this work, the use of a direct-introduction-type interface originally developed for the detection of non-volatile solutes in micro-LC with flame-photometric detection (FPD) [9,10] was coupled to a commercially available TID instrument. Technical aspects such as detector and interface modification and the optimization of the interface and TID parameters are discussed. Further, it is demonstrated that the system can handle non-volatile compounds in combination with both aqueous and organic LC eluents.

EXPERIMENTAL

Materials

All solvents were of HPLC grade from Merck (Darmstadt, Germany). PRP-X100 polymeric anion-exchange material, with a particle size of 10 μm (Hamilton, Reno, NV, USA), was used as the column packing material. Methylphosphonic acid (MPA), dimethyl methylphosphonate (DMMP) and dimethylphosphoric acid (DMP) were synthesized at the Prins Maurits Laboratory TNO. Glyphosate and dichlorvos were obtained from Dr. S. Ehrenstorfer (Augsburg, Germany).

Apparatus

The chromatographic system consisted of a Phoenix Model 20 CU pump (Carlo Erba, Milan, Italy), a Valco sample injection valve (VICI, Schenkon, Switzerland) with a 60-nl internal volume and a thermionic detector (Carlo Erba). The various fused-silica connection tubings (0.02–0.3 mm I.D.) were supplied by Chrompack (Middelburg, Netherlands).

The microcolumns (0.3 mm I.D., fused silica) were packed with PRP-X100 according to the procedure of Gluckman *et al.* [11]. The column performance was tested using a Spectroflow 783, UV detector (Kratos, Ramsey, NJ, USA) assembled with a laboratory-made 40-nl micro UV flow cell [12].

Detector modification. The thermionic detector (Fig. 1A) consists of four major parts: the detector base body (1) with insulation (a) and the glass burner tip (b); the actual detector (2), which contains the

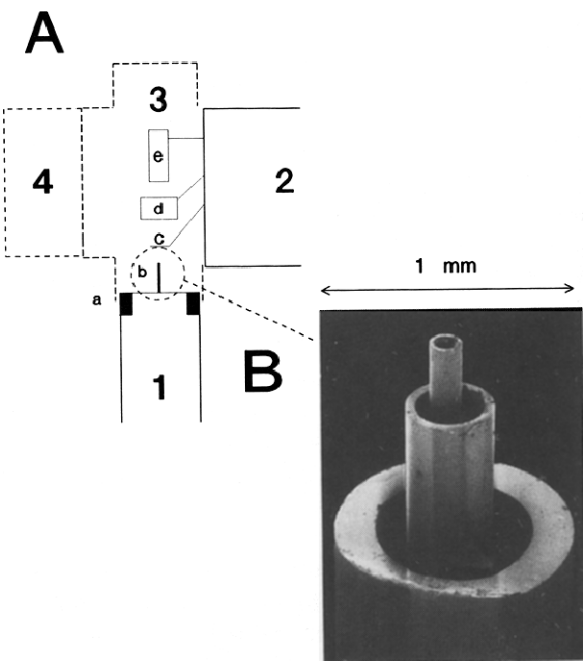

Fig. 1. (A) Thermionic detector used for micro-LC: 1 = base body with (a) insulation and (b) interface tip; 2 = actual detector which contains the electronics, (c) the electrode, (d) Rb source and (e) collector; 3 = detector housing; 4 = U-shaped aluminium block. (B) Interface tip with eluent introduction capillary (0.1 mm I.D. fused silica), fused-silica capillary (0.32 mm I.D.) providing the helium flow and 0.7 mm I.D. burner rim glass tube.

electronics, the electrode (c), the rubidium (Rb) source (d) and the collector (e); the aluminium detector housing (3), which covers the collector, the Rb source and electrode, and prevents atmospheric interferences during detector operation; and an external heating unit mounted in a laboratory-made U-shaped aluminium block (4).

In GC, the thermionic detector is heated via the detector base body which supports the housing and is placed in the heating unit of the gas chromatograph. To maintain liquid introduction when working in the LC mode, it is necessary to have a relatively cold detector base to prevent too early evaporation of the eluent. As a consequence, to avoid condensation of vapour, an external heating unit was mounted in a U-shaped aluminium block, which fits on to the detector housing. To prevent heat transfer from the housing to the base body, insulation (1, a) was inserted between both parts.

Burner head modification. The original metal flame jet also acts as a polarizing electrode and is therefore electrically insulated from the base body. Because of the direct flame contact and the insulation from the base body, the metal flame jet is probably too hot to maintain liquid flow when a 100 μm I.D. fused-silica capillary is put through the jet for LC effluent introduction. Clogging of the fused-silica capillary by non-volatile analytes occurred especially when working with relatively low-boiling eluents (60–100°C). Therefore, the flame jet was removed from the flame tip assembly, leaving an opening suitable for inserting a modified burner tip. The new glass burner tip was situated 6 mm above the base, *i.e.*, at the same height as the original flame jet. To prevent an electrical short-circuit between the electrodes and the top of the metal detector base, a 3-mm thick silicon ring was placed on top of the detector base.

Burner tip modification. The specially designed burner tip, developed in order to combine micro-LC with FPD [9], contains a 100 μm I.D. fused-silica (eluent introduction) capillary which is connected directly with the microcolumn. This capillary was placed in a 320 μm I.D. fused-silica capillary which is used for helium addition. Both capillaries were mounted in a 0.7 mm I.D. metal tube which is used for hydrogen addition. Modification of the metal tube of the FPD interface was necessary to prevent an electrical short-circuit between the electrodes and the interface: a glass tube (20 mm × 1.3 mm O.D. × 0.7 mm I.D.) was mounted with 1-cm shrinking Teflon on the end of the metal tube; this provides sufficient electrical insulation. Additionally, the use of glass prevents heat transfer to the lower part of the fused-silica LC eluent introduction capillary. The tip of the glass tube, which is also the burner rim, is shown in Fig. 1B. The hydrogen flow is introduced through the glass tube of the interface causing the flame to originate at the glass tube outlet. The original hydrogen flow inlet is, therefore, not used. The tip of the glass tube, *i.e.*, the burner rim, was used throughout this study as a reference point for measuring flame lengths, fused-silica tip positions and Rb source–burner rim distances.

The air flow was introduced through its original inlet mounted in the detector base.

Temperature measurement. Flame temperatures were measured with the use of a laboratory-made platinum *versus* platinum–10% rhodium thermocouple (2 mm × 0.1 mm O.D.) insulated with a 100 mm × 1.4 mm O.D. ceramic rod. The temperature range of this thermocouple extends to 1700°C as derived from standard calibration tables for thermocouples [13].

RESULTS AND DISCUSSION

Optimization of the total LC–interface–flame-based TID system with liquid LC eluent introduction into the diffusion flame is complicated because of the multivariate nature of the problem. Therefore, in this study, the optimization of the interface and the thermionic detector were considered separately. Further, one should realize that parameters such as the various gas flow-rates and the position of the Rb source and the eluent introduction capillary relative to the burner rim may all affect the analyte introduction into the flame. Therefore, a volatile test compound, DMMP, was selected which shows a TID response that is, to a first approximation, independent of the mode of introduction (liquid or vapour) and is therefore very suitable for studying the detector characteristics. The TID response of the corresponding free acid, MPA, on the other hand, will depend strongly on the mode of introduction and/or interface operation: MPA was therefore selected as a second test solute.

In order to study the influence of the different parameter settings on the analyte introduction visually, preliminary variation of each parameter was carried out with an open system, *i.e.*, without using the detector housing [see Fig. 1 (3)]. In this case the surrounding atmospheric air maintains a relatively constant hydrogen-to-oxygen (H_2:O_2) ratio in the flame owing to the high flammability of hydrogen [14]. Hence with the use of an open system the air flow-rate is eliminated as a parameter.

All open- and closed-system optimization studies were carried out using flow-injection analysis (10 μl/min) with methanol as carrier stream. Next, the total analytical system was tested under chromatographic conditions.

Optimization of interface

The influence of the liquid eluent and analyte introduction on the flame characteristics was the first parameter to be studied. A hydrogen flow-rate of 30 ml/min, as used in the GC mode of operation, results in a small flame only 2–3 mm high. This flame is too small to accept liquid flow-rates without causing flame instability. Therefore, it was elongated by increasing the hydrogen flow-rate until regular flame combustion was again obtained. The minimum flame length required to achieve this was about 6 mm; it needed a hydrogen flow-rate of *ca.* 60 ml/min.

The use of helium cooling is required to prevent overheating of the fused-silica tip, which becomes visible as glowing of the tip as a result of a vortex flow around the burner rim. On increasing the helium flow-rate, F, over the range 0–150 ml/min, a linear decrease in the tip temperature, T, was observed over the range 1100–500°C, *viz.*, $T = -4F + 1115$, with a correlation coefficient, r, of 0.996 ($n = 6$). According to our experience, under normal operating conditions, *i.e.*, when the detector housing is closed, helium flow-rates of less than 200 ml/min are preferred in order to avoid an unstable flame which is easily extinguished. At a helium flow-rate of *ca.* 100 ml/min the flame becomes colourless, indicating that direct contact of the flame with the glass burner tip is avoided and that cooling is efficient. This result is independent of the hydrogen flow-rate in the range tested, *viz.*, 40–300 ml/min.

The positions of the tip of the LC eluent introduction capillary and the helium-cooling capillary were varied relative to the burner rim position at fixed flow-rates of 60 ml/min of hydrogen and 100 ml/min of helium. The TID responses of DMMP and MPA were measured as a function of these fused silica outlet–burner rim positions. If the LC eluent introduction capillary protruded 5 mm or more above the burner rim, with the helium-cooling capillary at the same height as the burner rim, the non-volatile MPA could not be detected at all, while the volatile methyl derivative, DMMP, gave a constant high signal. Under these conditions, the interface probably operates in the evaporation mode, that is, effluent evaporation is complete, which causes the non-volatile MPA to be deposited in the capillary. For lower positions of the tip of the LC eluent introduction capillary, *i.e.*, for protruding distances from 5 to 0 mm above the burner rim, the MPA signal increased. For tip positions of 0–0.5 mm, the same signal was found for both test compounds. It was also found that the tip of the helium-cooling capillary should not protrude further than the LC eluent introduction capillary; it was positioned *ca.* 0.2–0.3 mm above the burner rim.

Obviously, the introduction of non-volatile test compounds into the flame is complete when the LC eluent introduction capillary outlet is positioned close to the burner rim and just above the tip of the capillary through which the helium gas flow exits.

Optimization of TID

Initial experiments with the open detector system were carried out in order to measure more accurately the distances between the Rb source and burner rim and, additionally, to verify the eluent and analyte introduction stability. The hydrogen and helium flow-rates were 80 and 100 ml/min, respectively. The optimum Rb source–burner rim distance was found to be 7 mm. Optimum signal-to-noise ratios (S/N) for both MPA and DMMP were obtained with the flame coming very close to the Rb source without enveloping it (as indicated by glowing of the Rb source). In the latter situation, the noise level increased dramatically.

Next, the Rb source–burner rim distance was set at 7 mm and the hydrogen flow-rate was varied between 60 and 130 ml/min. With the free acid MPA it was observed that solute introduction remained stable without clogging of the LC eluent introduction

capillary for a hydrogen flow-rate of at least 60 ml/min. The S/N was maximum at *ca.* 80 ml/min. The mutual dependence of the optimum source–rim distance and hydrogen flow-rate was demonstrated by slightly increasing the hydrogen flow-rate, *i.e.* by 10–15 ml/min; this immediately resulted in a 25-fold increase in the noise level. However, on increasing the Rb source–burner rim distance (by *ca.* 0.5 mm), the earlier low noise level was again obtained and the S/N was restored to its original value. The result was found to be independent of the introduction of additional air via the detector base, as was to be expected on the basis of the high flammability of hydrogen in (ambient) air.

Next, the detector was closed and the air flow-rate was varied over the range 120–300 ml/min. On the basis of the S/N, the optimum air flow-rate was found to be 200 ml/min. Compared with the open system discussed above, the S/N increased 15-fold owing to the reduced noise level. The lower noise level observed with the closed system is probably due to the absence of dust particles which are abundantly present in the laboratory atmosphere. This agrees with findings of McWilliam [15] in his early studies on the use of the flame ionization detector for GC. With the closed system and the above conditions, an optimum source–rim position similar to the above, *viz.*, 7–8 mm, was found for both analytes (Fig. 2).

Two-parameter studies. The combined influence of the air flow-rate and the Rb source position on analyte signal, noise and background at constant hydrogen flow-rate, expressed as H_2:O_2 ratio, was studied using methanol as carrier stream (Fig. 3). It is evident from the data that signal (Fig. 3A), noise (Fig. 3B) and background (Fig. 3C) all reach maximum values when the H_2:O_2 ratio is about 2, *i.e.*, is near-stoichiometric. Although the essentially similar profiles of analyte signal and noise plots suggest the lack of a distinct optimum S/N, closer observation reveals that such an optimum does exist in the H_2:O_2 range 1.9–2.1 (Fig. 4).

For a more exact determination of the above optimum, experiments were carried out using calibrated hydrogen and air flow-rates. With hydrogen

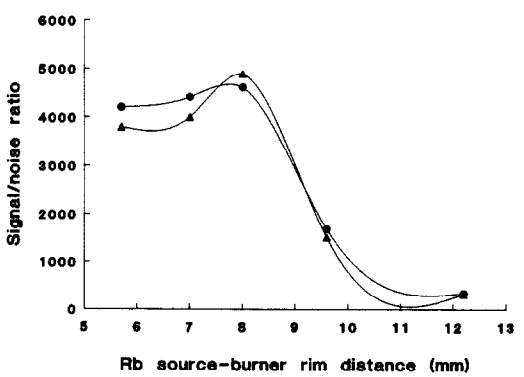

Fig. 2. Dependence of signal-to-noise ratio on Rb source–burner rim distance. Analytes: ▲ = DMMP; ● = MPA. Flow-rates: hydrogen, 80 ml/min; air, 200 ml/min; helium, 100 ml/min. Eluent: methanol at 10 μl/min.

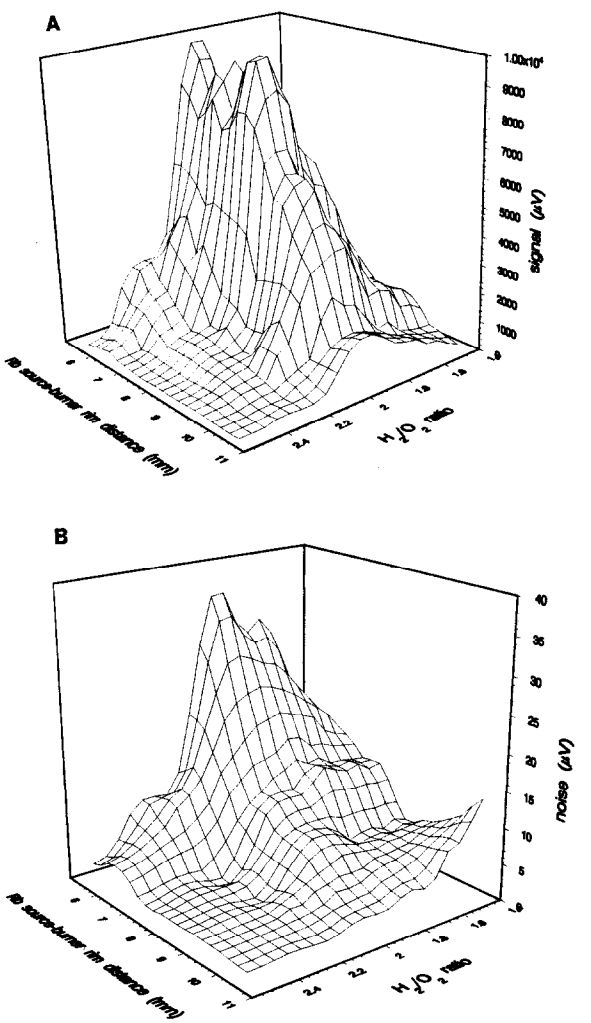

Fig. 3.

(Continued on p. 64)

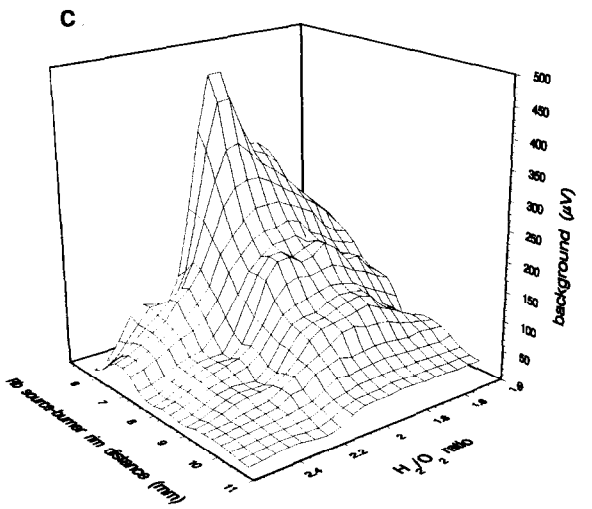

Fig. 3. Dependence of (A) signal, (B) noise and (C) background on Rb source–burner rim distance and H_2:O_2 ratio. Flow-rates: hydrogen, 125 ml/min; helium, 100 ml/min. Eluent: methanol at 10 μl/min. Analyte: DMMP.

flow-rates of 78, 88, 110 and 118 ml/min and varying air flow-rates, maximum S/N values were found at 200, 225, 280 and 304 ml/min of air, respectively, *i.e.*, at stoichiometric H_2:O_2 ratios of 1.95 ± 0.01. In daily practice, an elegant experimental method to find the optimum air flow-rate is to start with an excess of hydrogen and then to increase the air flow-rate slowly up to the level where the background (see Fig. 3C) just starts to increase.

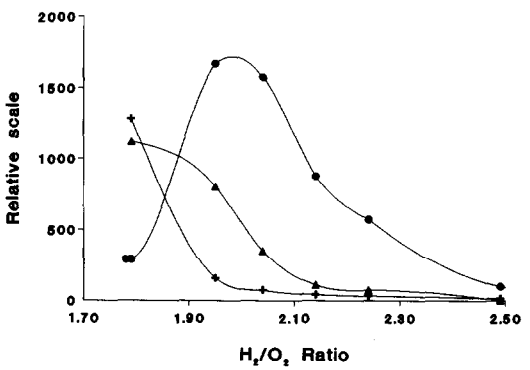

Fig. 4. Dependence of (▲) signal, (+) noise and (●) signal-to-noise ratio on H_2:O_2 ratio (cross-section of Fig. 3 at Rb source–burner rim distance of 8 mm). Flow-rates: hydrogen, 125 ml/min; helium, 100 ml/min. Eluent: methanol at 10 μl/min. Analyte: DMMP.

Next, the combined influence of the Rb source–burner rim distance and the hydrogen flow-rate was studied at a constant H_2:O_2 ratio of 1.95. DMMP was used as test compound and methanol as carrier stream. As is shown in Fig. 5A, the analyte signal increased on decreasing the source–rim distance, especially when working at higher hydrogen (and of course, air) flow-rates. Nevertheless, the best S/N values were obtained at relatively large source–rim distances of 7–12 mm, the exact value depending on

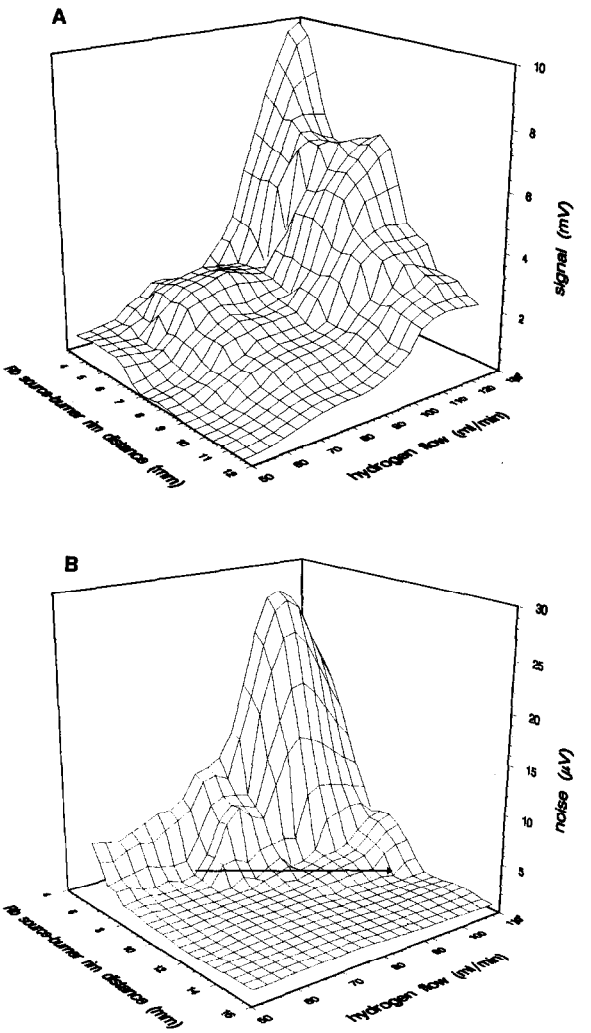

Fig. 5. Dependence of (A) signal and (B) noise on Rb source–burner rim distance and hydrogen flow-rate. H_2:O_2 ratio, 1.96; helium flow-rate, 100 ml/min. Eluent: methanol at 10 μl/min. Analyte: DMMP.

both the hydrogen and air flow-rates. This can be explained by the noise profile shown in Fig. 5B. As a consequence, the best S/N values are obtained by following the arrow drawn in the latter figure.

Influence of the carrier stream. The influence of the methanol flow-rate was studied with the Rb source–burner rim distance set at 8 mm and the H_2:O_2 ratio at 1.95 (80 ml/min of hydrogen and 200 ml/min of air). The methanol flow-rate was varied between 3 and 15 μl/min. As is evident from Fig. 6, a distinct S/N optimum occurs for both DMMP and MPA at a methanol flow-rate of 10 μl/min. Because the flame length depends on the (combustible) methanol flow-rate, as will be shown in Part II [16], a flow-rate of 10 μl/min was applied throughout this study.

As it is our aim to set up an on-line LC–interface–TID system, finally the nature of the carrier stream was varied. The S/N level for DMMP remained essentially the same when hexane was used instead of methanol as the LC carrier stream. However, when water was used as solvent, also at the flow-rate of 10 μl/min, the baseline became less stable and an increase in the noise level by a factor of 4 was observed. The baseline instability was found to be due to irregular solvent introduction into the flame and will be discussed in more detail in Part II [16]. The detector noise could be reduced and stable carrier stream introduction restored by an increase of 0.5 mm in the distance between the LC eluent introduction capillary and the burner rim. These findings are in agreement with our results on the use of the micro-LC–FPD system with aqueous LC eluents [9].

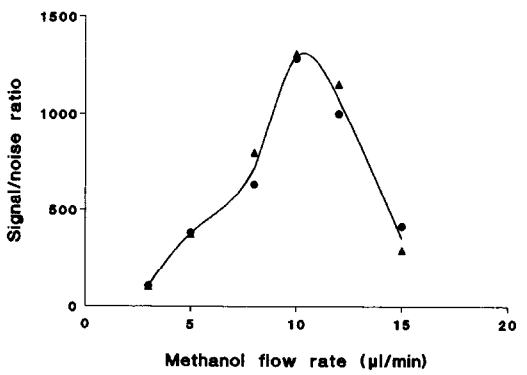

Fig. 6. Dependence of signal-to-noise ratio on methanol flow-rate. Test compounds: ● = DMMP; ▲ = MPA. For further conditions, see text.

With water instead of methanol, the experiment in Fig. 3 was repeated, *i.e.*, the Rb source–burner rim distance and the H_2:O_2 ratio were simultaneously varied, while maintaining a constant hydrogen flow-rate. In contrast to the results with methanol, with water the background current remained low (< 150 pA) and the noise essentially constant (3 ± 1 μV), independent of the Rb source–rim distance and the air flow-rate. This essentially different situation results in a less complicated optimization which is exclusively based on the TID response observed. The influence of water on the signal was essentially the same as with methanol (data not shown), *e.g.*, a maximum occurred at an H_2:O_2 ratio of *ca.* 2; the steep decrease at smaller Rb source–burner rim distances of less than 7 mm was not observed, however, with methanol, where the noise and signal keep increasing (see Fig. 5A and B). This explains that the maximum S/N values were found to be essentially the same with both solvents. However, under the same gas flow and carrier stream conditions, the optimum source–rim distance is 7 mm with water and 9 mm with methanol. This will be discussed in more detail below.

For the separation of inorganic phosphorus-containing acids or acidic organophosphorus compounds, which typically are target components for our LC–interface–TID system, aqueous LC eluents to which volatile acids or salts have been added are usually necessary. Therefore, the optimization of the system was repeated using a micro PRP-X100 anion-exchange column and aqueous–organic eluents containing organic acids or salts. On the basis of the above results, the detector parameters were set as indicated in Table I.

The influence on the TID performance of both the Rb source–burner rim distance and the percent-

TABLE I

PARAMETER SETTINGS FOR MICRO-LC–INTERFACE–TID

Parameter	Value
Hydrogen flow-rate	120 ml/min
Air flow-rate	300 ml/min
Helium flow-rate	100 ml/min
Rb source–burner rim distance	Varied
LC eluent flow-rate	10 μl/min

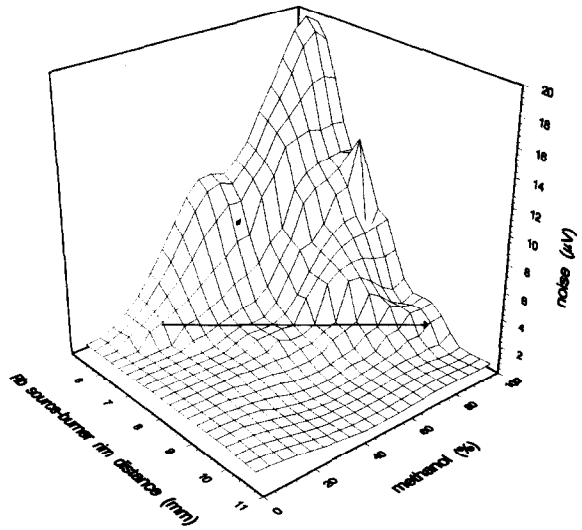

Fig. 7. Dependence of noise on Rb source–burner rim distance and percentage of methanol in LC eluent. Hydrogen flow-rate, 125 ml/min; H_2:O_2 ratio, 1.96. Helium flow-rate, 50 ml/min. Eluent: aqueous 0.6% formic acid, with varying methanol content (0–100%); flow-rate, 10 μl/min.

age of methanol in the aqueous 0.6% formic acid used as the LC eluent was studied. The data presented in Fig. 7 show that on increasing the methanol content from 0 to 95% (v/v) the noise increases dramatically. The three-dimensional plot in Fig. 7 helps to explain the different optimum Rb source–burner rim distances of *ca.* 7 and 9 mm found experimentally when using water and pure methanol as carrier stream, respectively. As discussed above, the most striking difference between the use of water and methanol is the constancy of the noise observed with the former solvent, irrespective of the Rb source–burner rim distance and/or the H_2:O_2 ratio (at a constant hydrogen flow-rate) selected. In other words, on increasing the percentage of methanol in the eluent, the noise will increase and the optimum S/N values will be found when following the full line in Fig. 7. To a first approximation, this line indicates the optimum Rb source–burner rim distance for each methanol–water eluent composition.

Electrode collector polarization. For GC analysis, the manufacturers recommend that the thermionic detector be used with a −300 V polarization electrode potential, with +300 V as an alternative. Both options were studied using 60-nl injections of *ca.* 7 mg/ml of DMMP in methanol. The less conventional positive electrode potential resulted in a six-fold increased S/N ratio compared with the negative electrode potential. The background measured relative to that without LC eluent introduction was the same in both experiments (*ca.* 20 nA). It was decided to use the positive polarization mode in all further work.

TABLE II

INFLUENCE OF ELUENT COMPOSITION ON THERMIONIC DETECTOR NOISE

Eluent: methanol–water (100:0 → 0:100) with or without added (I) ammonium oxalate, (II) ammonium acetate or (III) formic acid.

LC eluent				Noise (μV) at Rb source–burner rim distance of		
Methanol (%)	I (*M*)	II (*M*)	III (*M*)	7.5 mm	8.5 mm	9.5 mm
0				2.0	1.6	1.8
0			0.11	1.6	1.6	1.6
0	0.15			1.6		
0		0.25		1.5		
30			0.11	1.5		
50			0.11	2.0	0.2	0.2
60		0.05				0.4
70		0.15				1.7
80		0.05				0.6
90		0.05				0.5
95		0.05				0.3
95			0.11	4.9	2.3	0.2
100				5.3		0.01

TABLE III

DETECTION LIMITS (pg/s) OF ANALYTES IN MICRO-LC–TID

Eluent[a]				Analyte[b]		
M	W	F	A	MPA	DMMP	DMP
0	100	0.5	–	140	160	–
50	50	0.5	–	90	100	80
80	20	0.3	0.2	90	–	100
100	–	–		45	50	50

[a] Composition in vol.%: M, methanol; W, water; F, formic acid (98–100%); A, ammonia (25%).
[b] MPA, methylphosphonic acid; DMMP, dimethyl methylphosphonate; DMP, dimethylphosphoric acid.

Analytical data

Detector noise. The detector noise under different eluent conditions and Rb source–burner rim distances is shown in Table II. The noise level is seen to be essentially constant at a methanol concentration of 60–95% with or without 0.05 *M* ammonium acetate added. The noise level increases by at least a factor of 3 when the salt concentration is increased to 0.15 *M*. Similar noise levels in the range 1.5–2.0 μV are observed in pure water and for low modifier contents (0–30% methanol), also in the presence of salts (ammonium oxalate or ammonium acetate). Obviously, the system is suitable for both reversed-phase and ion-exchange chromatography, provided that the ionic strength of the eluent is relatively low. At higher modifier contents (30–100%) the noise depends on the Rb source–burner rim distance as discussed above. The lowest noise level was observed when using pure methanol as an eluent at the optimum Rb source–rim distance of *ca.* 9 mm.

Detector sensitivity. The sensitivity of the micro-LC–TID system was studied by injecting solutions of DMMP, MPA and DMP in various eluents. The detection limits of the analytes determined at S/N = 2 are summarized in Table III. The results indicate that the micro-LC–TID system is more suitable for use with organic than with aqueous eluents. The detection limits in aqueous eluents containing ammonia or formic acid generally are about double those obtained with micro-LC–FPD [12]. With pure methanol as eluent, and also with hexane [17], the micro-LC–TID system shows a sensitivity of 10–20 pg/s of phosphorus, which is similar to that of the micro-LC–FPD system. Compared with GC or supercritical fluid chromatography [18], there is, however, a loss of sensitivity of about two orders of magnitude. This is a result of the 100-fold higher noise level caused by the introduction of the LC eluent.

Applications

The applicability of the system was tested by separating and detecting polar organophosphorus compounds such as DMP and glyphosate. These compounds are difficult to analyse because they are highly polar, and therefore difficult to extract from aqueous samples or biological fluids, and non-volatile; in addition, they do not possess suitable chromophores or fluorophores. The increasing use of biodegradable organophosphorus pesticides has stimulated interest in the determination of their degradation products or metabolites. The primary breakdown products are substituted dialkyl(thio) organophosphorus acids.

DMP is the major and most hydrophilic metabolite in animals of a number of commercially available insecticides including dichlorvos (DDVP) [19], monocrotophos and mevinphos [20]. Generally, GC is used after laborious isolation, clean-up and diazoalkane derivatization [21,22]. With the micro-LC–TID system DDVP and DMP can be simultaneously determined without previous derivatization, *viz.*, on a PRP-X100 fused-silica capillary column. Owing to the hydrophobic and strong anion-exchange properties of the packing material, the compounds can be separated with an eluent containing 93% methanol and 0.5 *M* ammonium acetate (Fig. 8).

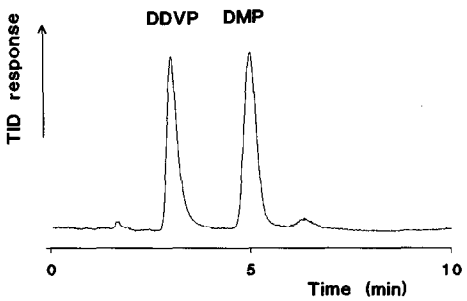

Fig. 8. Micro-LC–TID separation of dichlorvos (DDVP) and its major metabolite DMP. Column: PRP-X100 (200 mm × 0.32 mm I.D.). Eluent: methanol–0.05 *M* ammonium acetate (93:7) at 10 μl/min.

Glyphosate is a broad-spectrum herbicide marketed by Monsanto under the trade name Roundup. It has widespread application, *e.g.*, for potatoes, wheat, barley and asparagus. In soil the residual herbicide is readily adsorbed on soil particles where it undergoes microbial degradation to ammonia and carbon dioxide [23]. Extraction using organic solvents is an onerous task because of its polar and amphoteric character; the best results are obtained with water [24]. Determination is done by GC after extensive clean-up and derivatization [23–27] or by LC after pre- or post-column derivatization [28–33]. The practicality of direct analysis is demonstrated in Fig. 9 for an aqueous soil extract which was spiked with *ca.* 1 ppm of glyphosate. After filtration, 2 μl of the extract were injected directly on to the PRP-X100 column using methanol–water–formic acid (30:70:1) as eluent. The example shows that a large-volume injection of 2 μl has no adverse effects on system performance: the glyphosate peak shape is satisfactory. This may be explained by a focusing effect of the sample solution. The spikes just after the glyphosate peak are caused by a small amount of air which was introduced during injection. The detection limit of the herbicide in soil was 200 ppb under the present conditions.

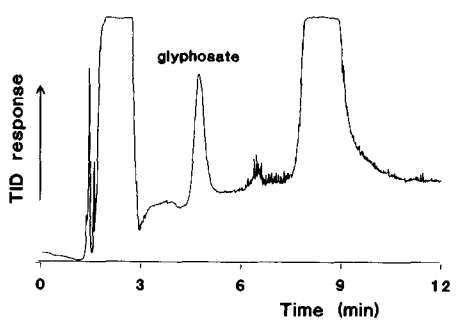

Fig. 9. Micro-LC–TID separation of an aqueous soil extract spiked with 1 ppm of glyphosate. Column: PRP-X100 (150 mm × 0.32 mm I.D.). Eluent: methanol–water–formic acid (30:70:1) at 10 μl/min. Amount injected: 2 μl.

CONCLUSIONS

The systematic study of the present micro-LC–TID system has shown that careful optimization of the various gas flow-rates and of the Rb source position is required. The H_2:O_2 ratio should be near-stoichiometric, with the exact value depending slightly on the type of eluent used, and the flame length should be at least *ca.* 6 mm. The micro-LC–TID system can be used with purely organic and with aqueous solvents. In addition, the presence of salt concentrations of up to 0.2 *M* can be tolerated. Under suitable chromatographic conditions detection limits of about 100 pg/s of analyte can be obtained for alkylphosphonic and alkylphosphoric acids. As an application, the simultaneous determination of organophosphorus pesticides and their polar (acidic) degradation products has been reported.

ACKNOWLEDGEMENT

The authors are grateful to Bart Zegers for experimental assistance and helpful discussions.

REFERENCES

1 U. A. Th. Brinkman and F. A. Maris, *LC · GC Int.*, 1 (1987) 45.
2 F. A. Maris, R. J. van Delft, R. W. Frei, R. B. Geerdink and U. A. Th. Brinkman, *Anal. Chem.*, 58 (1986) 1634.
3 J. C. Gluckman, D. Barcelo, G. J. de Jong, R. W. Frei, F. Maris and U. A. Th. Brinkman, *J. Chromatogr.*, 367 (1986) 35.
4 D. Barcelo, F. A. Maris, R. W. Frei, G. J. de Jong and U. A. Th. Brinkman, *Int. J. Environ. Anal. Chem.*, 30 (1987) 95.
5 V. L. McGuffin and M. Novotny, *Anal. Chem.*, 55 (1983) 2296.
6 J. C. Gluckman and M. Novotny, *J. Chromatogr.*, 314 (1984) 103.
7 J. C. Gluckman and M. Novotny, *J. Chromatogr.*, 333 (1985) 291.
8 Ch. E. Kientz and A. Verweij, *Int. J. Environ. Anal. Chem.*, 30 (1987) 255.

9 Ch. E. Kientz, A. Verweij, H. L. Boter, A. Poppema, R. W. Frei, G. J. de Jong and U. A. Th. Brinkman, *J. Chromatogr.*, 467 (1989) 385.
10 Ch. E. Kientz, A. Verweij, G. J. de Jong and U. A. Th. Brinkman, *J. High Resolut. Chromatogr.*, 12 (1989) 793.
11 J. C. Gluckman, A. Hirose, V. L. McGuffin and M. Novotny, *Chromatographia*, 17 (1984) 3039.
12 Ch. E. Kientz and A. Verweij, *J. High Resolut. Chromatogr. Chromatogr. Commun.*, 3 (1988) 294.
13 D. R. Lide (Editor), *CRC Handbook of Chemistry and Physics*, CRC Press, Boca Raton, FL, 72nd ed., 1991–92, p. 15-1.
14 R. A. Strehlow (Editor), *Fundamentals of Combustion*, Robert E. Kreiger Publishing, Huntington, NY, 1979.
15 I. G. McWilliam, *Chromatographia*, 17 (1983) 241.
16 Ch. E. Kientz, A. Verweij, G. J. de Jong and U. A. Th. Brinkman, *J. Chromatogr.*, 626 (1992) 71.
17 Ch. E. Kientz, J. P. Langenberg, G. J. de Jong and U. A. Th. Brinkman, *J. High Resolut. Chromatogr. Chromatogr. Commun.*, 7 (1991) 460.
18 J. G. J. Mol, B. N. Zegers, H. Lingeman and U. A. Th. Brinkman, *Chromatographia*, 32 (1992) 203.
19 D. H. Hutson and E. C. Hoadley, *Xenobiotica*, 2 (1972) 107.
20 K. I. Beynon, D. H. Hutson and A. N. Wright, *Residue Rev.*, 47 (1973) 55.
21 M. T. Shafic, D. E. Bradway, H. F. Enos and A. R. Yobbs, *J. Agric. Food Chem.*, 21 (1973) 625.
22 D. Blair and H. R. Roderick, *J. Agric. Food Chem.*, 24 (1976) 1221.
23 M. L. Rueppel, B. B. Brigtwell, J. Schaefer and J. T. Marvel, *J. Agric. Food Chem.*, 25 (1977) 517.
24 R. A. Guinivan, N. P. Thompson and W. B. Wheeler, *J. Assoc. Off. Anal. Chem.*, 65 (1982) 35.
25 J. N. Seiber, M. M. McChesney, R. Kon and R. A. Leavitt, *J. Agric. Food Chem.*, 32 (1984) 681.
26 C. L. Deyrub, S. Chang, R. A. Weintraub and H. A. Moye, *J. Agric. Food Chem.*, 33 (1985) 944.
27 R. N. Dibyendu and K. K. Samir, *J. Agric. Food Chem.*, 37 (1989) 441.
28 H. Roseboom and C. J. Berkhoff, *Anal. Chim. Acta*, 135 (1982) 373.
29 R. L. Glass, *J. Agric. Food Chem.*, 31 (1983) 280.
30 H. A. Moye, C. J. Miles and S. J. Scherer, *J. Agric. Food Chem.*, 31 (1983) 69.
31 T. E. Archer and J. D. Stokes, *J. Agric. Food Chem.*, 32 (1984) 586.
32 J. E. Cowell, J. L. Kunstman, P. J. Nord, J. R. Steimetz and G. R. Wilson, *J. Agric. Food Chem.*, 34 (1986) 955.
33 L. G. M. Th. Tuinstra and P. G. M. Kienhuis, *Chromatographia*, 24 (1987) 696.